Tunnelling and Underground Space Technology 54 (2016) 81–91

Contents lists available at ScienceDirect

Tunnelling and Underground Space Technology

journal homepage: www.elsevier.com/locate/tust

Stability analysis of underground oil storage caverns by an integrated numerical and microseismic monitoring approach

K. Ma [a,b], C.A. Tang [c], L.X. Wang [d], D.H. Tang [a], D.Y. Zhuang [c], Q.B. Zhang [e,*], J. Zhao [e]

[a] Institute of Mechanics, Chinese Academy of Sciences, Beijing 100190, China
[b] Dalian Mechsoft Co., Ltd., Dalian, Liaoning 116600, China
[c] The State Key Laboratory of Coastal and Offshore Engineering, Dalian University of Technology, Dalian, Liaoning 116024, China
[d] CAEP Software Center for High Performance Numerical Simulation, Institute of Applied Physics and Computational Mathematics, Beijing 100088, China
[e] Department of Civil Engineering, Monash University, VIC 3800, Australia

ARTICLE INFO

Article history:
Received 13 October 2015
Received in revised form 14 January 2016
Accepted 15 January 2016
Available online 8 February 2016

Keywords:
Underground storage caverns
Continuous–Discontinuous Element Method (CDEM)
Numerical simulation
Microseismic monitoring
Stability analysis
Excavation unloading

ABSTRACT

Underground storage in unlined caverns is of great significance for storing energy resources. Construction of underground storage caverns is an extremely complex process, involving extensive multi-bench excavation and strong unloading. Excavation-induced damage of surrounding rock masses may lead to instability of underground storage caverns. The aim of this paper is to put forward a method by integrating numerical simulation and microseismic monitoring for evaluation of cavern stability. A novel numerical method called Continuous–Discontinuous Element Method (CDEM) is applied to simulate micro-cracks under excavation-induced unloading conditions. Meanwhile, a microseismic (MS) monitoring system is employed to monitor real-time MS events during construction of storage caverns. Numerical results are validated using the monitoring data from the MS monitoring system. The integrated method is proved to be successful in capturing micro-cracks in underground storage caverns. Local instability, potential unstable zones and micro-crack evolution are analyzed, and cracking mechanisms are also discussed.

1. Introduction

Underground storage in unlined caverns has numerous advantages over aboveground storage (Morfeldt, 1974; Bergman, 1984; Broms and Zhao, 1993; Zhao et al., 1996, 1999, 2004; Sun and Zhao, 2010; Rutqvist et al., 2012), for instance, larger storage capacity, longer service life, and less resource consumption. Meanwhile, the underground storage is safe from extreme conditions such as fire, earthquake and explosion. For oil storage caverns, the sealing effects of groundwater reduce the risk of oil leakage toward the surrounding rock mass (Kiyoyama, 1990). Therefore, underground storage caverns have been popular in various countries for storing strategic energy resources (Morfeldt, 1983; Kiyoyama, 1990; Lee and Song, 2003; Benardos and Kaliampakos, 2005; Li et al., 2014), including crude oil (Kiyoyama, 1990), liquefied petroleum gas (LPG) (Yang and Guan, 2001) or liquefied natural gas (LNG) (Lee et al., 2006). Whichever kind of energy resources are stored in the underground storage caverns, two fundamental principles should be strictly followed. The first one is that the groundwater pressure around caverns should be higher than that of the stored energy resource so as to prevent its migration (Åberg, 1977; Thunvik and Braester, 1980; Goodall et al., 1988; Lindblom, 1997; Yang et al., 2004; Sun and Zhao, 2010; Sun et al., 2011; Li et al., 2014). The other is the stability of rock masses around caverns (Lindblom, 1997; Lu, 1998; Ibrahim et al., 2015).

However, high sidewalls and large spans of caverns, and uncertain discontinuities in the surrounding rock masses are often encountered, which seriously threaten the stability of underground caverns (e.g., Zhu and Zhao, 2004; Zhu et al., 2010). Many studies have been conducted on the stability of underground storage caverns during the construction phase. Gnirk and Fossum (1979) established a numerical model for the assessment of cavern stability of compressed air energy storages using probabilistic design procedures. Lindblom (1997) addressed rock stability by developing criteria to ascertain the full operation integrity of underground caverns. Tezuka and Seoka (2003) analyzed the stability of the surrounding rock masses of large-cross-section underground oil storage caverns in earthquake-prone Japan. Park et al. (2005) carried out geophysical investigations and numerical analyses for the stability assessment of the first LPG storage terminal constructed underneath a lake in western Korea. Yang et al. (2014) investigated the anisotropic properties of rock masses with consideration of the seepage-stress coupling effect. Nevertheless, there is no universal

* Corresponding author.
E-mail address: qianbing.zhang@monash.edu (Q.B. Zhang).

http://dx.doi.org/10.1016/j.tust.2016.01.024
0886-7798/

understanding on the stability mechanism of underground storage caverns due to uncertainties on geological structures and rock properties. With gradual expansion of underground storage caverns, the stability of surrounding rock masses during excavation becomes the key to the success of an underground storage cavern project. The unloading effect during excavation has great impact on the stability of underground storage caverns. Thus, integrated methods are necessary to analyze the stability and damage mechanism of underground storage caverns during construction. Continuous numerical approaches, such as finite difference method (FDM) (Narasimhan and Witherspoon, 1976), finite element method (FEM) (Koyama et al., 2009) and Boundary Element Method (BEM) (Mohanty and Vandergrift, 2012) have been extensively applied for stability analysis for underground storage caverns to deal with continuum-based problems (e.g. Preece and Foley, 1983; Lu, 1998; Heusermann et al., 2003; Mandal et al., 2013; Wang et al., 2015b). Discontinuous methods, for instance, discrete element method (DEM) (Cundall, 1971; Cundall and Strack, 1979), and discontinuous deformation analysis (DDA) (Shi, 1988), are useful to analyze discontinuities of rock masses (e.g. Zhao et al., 1999; Nadimi et al., 2011; Chen et al., 2013; Li et al., 2014; He and Zhang, 2015). However, studies involving the damage and failure evolution of the surrounding rock masses of the storage caverns have seldom reported. A motivation is to combine advantages of both continuous and discontinuous approaches proposed by Munjiza et al. (1995), Li et al. (2004), Wang et al. (2013), etc. These combined methods include FDEM (FEMDEM) (Munjiza et al., 1995; Munjiza, 2004; Mahabadi et al., 2010, 2012; Lisjak et al., 2014, 2015) and Continuous–Discontinuous Element Method (CDEM) (Li et al., 2004, 2008; Ma et al., 2011; Wang et al., 2013; Li et al., 2015). In the study of Cai et al. (2007), the continuum-based software FLAC was coupled with the discontinuum-based software PFC to investigate acoustic emissions in large-scale underground excavations. Lisjak et al. (2015) used the FDEM method to model the crack evolution due to the excavation of a circular tunnel in a bedded argillaceous rock. The progressive failure of rock masses was simulated by a cohesive-zone approach (Munjiza et al., 1995; Munjiza, 2004; Mahabadi et al., 2010, 2012; Lisjak et al., 2014, 2015). The method of CDEM not only can deal with both continuous and discontinuous problems, but also can reproduce the progressive damage and failure evolution of materials from a continuous state to a discontinuous state (Li et al., 2015). In the present study, CDEM is employed to simulate the excavation process of underground storage caverns.

Microseismic (MS) monitoring techniques have been successfully used to accurately and effectively monitor the micro-cracks within surrounding rock masses in many engineering projects (e.g., Hong et al., 2006; Kaiser, 2009; Tang et al., 2011; Xu et al., 2011; Ma et al., 2013; Cai et al., 2015; Feng et al., 2015, 2016). In this study, an advanced Microseismic Monitoring System (Engineering Seismology Group, Canada) is applied, which consists of microseismic sensors installed in rock masses, a Paladin data acquisition system and a data analysis center. Meanwhile, MS monitoring are used to verify CDEM results.

In this paper, two adjacent oil storage caverns are investigated to understand damage mechanisms of surrounding rock masses during the construction phase. The main objectives include modeling the damage process of the surrounding rock masses, validating CDEM results by M monitoring data, and analyzing the stability of underground storage caverns.

2. Project overview

2.1. Project layout

An underground water-sealed storage cavern project is selected for stability analysis with an integrated numerical and MS monitoring method. This project located in Jinzhou, Liaoning Province, China, was designed to have a total capacity of 300×10^4 m^3 for crude oil. It consists of eight storage caverns, namely 1N–4N and 1S–4S (see Fig. 1), which are located more than 100 m below the ground surface. The top of the caverns is located at −53 m ACD, and the bottom at −76 m ACD (where m stands for meter and ACD is the abbreviation of Admiralty Chart Datum). The cross section of each cavern has a dimension of 19 m in width and 24 m in height. The caverns are 946 m long along the East-West axis. The distance between two adjacent caverns is 48 m. In this paper, the construction process of 1N and 1S oil storage caverns is studied to analyze the damage mechanism of surrounding rock masses and thus to evaluate the stability of caverns.

2.2. Engineering geology

The ground surface is covered by residual soil while the bedrock consists of coarse and medium grained granite, according to site investigation and lab experiments. There are no large-scale fractures found within 10 km from the site. However, there are some diabase, aplite and diorite dikes (see Fig. 2), trending mainly in

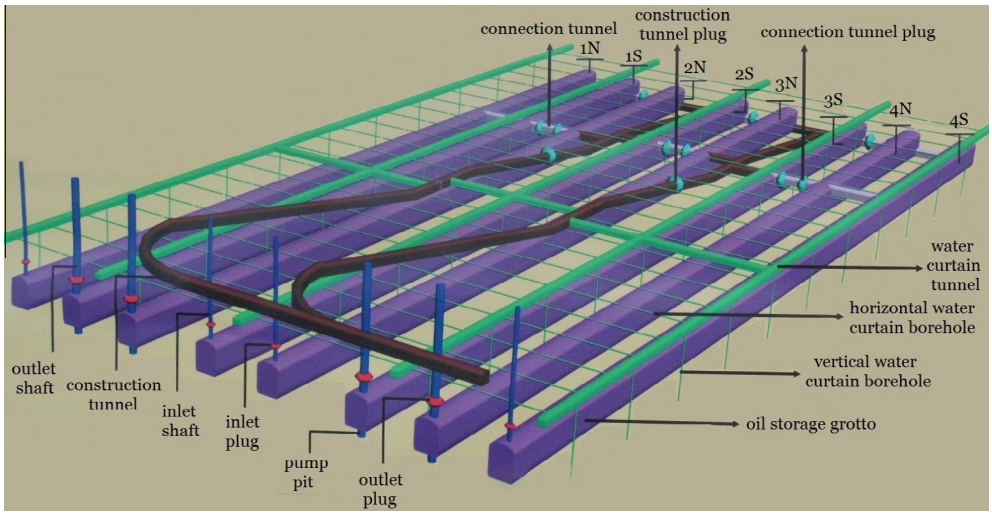

Fig. 1. Layout of the Jinzhou water-sealed underground storage caverns project.

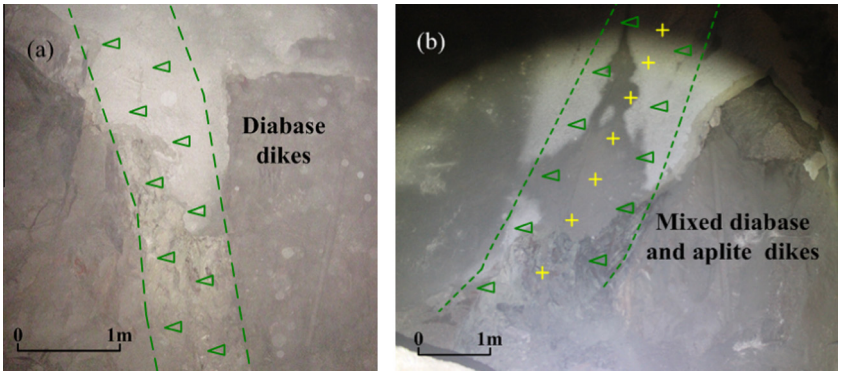

Fig. 2. Diabase dikes found at (a) Chainage 2 + 45 in Cavern 1N and (b) Chainage 2 + 80 in Cavern 1S.

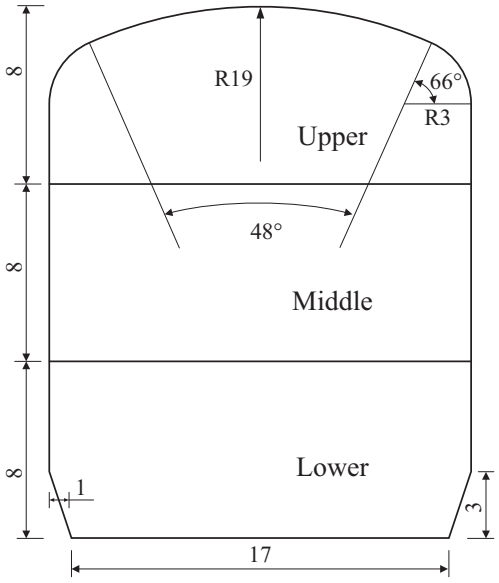

Fig. 3. Cross section of the underground storage cavern (unit: m).

NNW and NNE, with dip angle mostly ranging from 70° to 80° or from 40° to 50°. Joints were formed near dikes due to hydrothermal alteration. The groundwater mainly exists in the fracture network and fissure veins.

2.3. Excavation process

Due to the large cross section of storage caverns, a three-stage controlled blasting method was selected for excavation. These storage caverns were sequentially excavated from the upper bench to the middle and then to the lower (see Fig. 3). Each bench was 8 m high and was excavated with specific method according to rock classification. The upper, middle and lower benches were excavated simultaneously with a certain staggered distance to ensure safety. Excavation blasting for the middle bench took place every three or four days with a depth of 10 m and a volume of 4000 m^3. The excavation depth of the lower bench was around 5–10 m/d. The multi-bench excavation was featured by rapid and extensive excavation and strong unloading.

3. Fundamentals of Continuous–Discontinuous Element Method (CDEM)

The governing equations of CDEM are referred to Jing and Stephansson (2007), which includes dynamic equilibrium equations, linear elastic constitutive equations and displacement–strain relations.

3.1. Computational model

The computational domain is discretized into finite elements, which can be continuous, discontinuous or partially continuous. These three states correspond to the FEM, DEM and CDEM domains, respectively, as shown in Fig. 4, which are used to solve different types of problems. Conventionally, the FEM domain is used for fully continuous problems, while the DEM domain for fully discontinuous problems. The CDEM domain can be used to simulate the evolution of rock masses from a continuous state to a discontinuous state by breakage of contact interfaces, according to the maximum tensile strength criterion or Mohr-Coulomb law (Li et al., 2007).

As shown in Fig. 5, there are two kinds of elements in CDEM, i.e. blocks and contacts, and thus CDEM is basically a combination of FEM and DEM. FEM is used to compute stresses within the block,

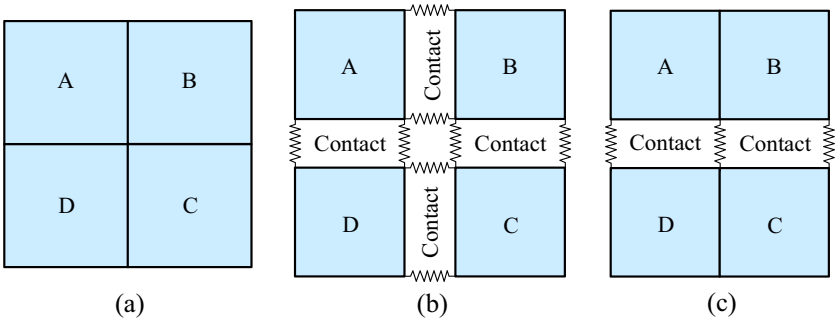

Fig. 4. Comparison of computational domains: (a) FEM, (b) DEM, and (c) CDEM.

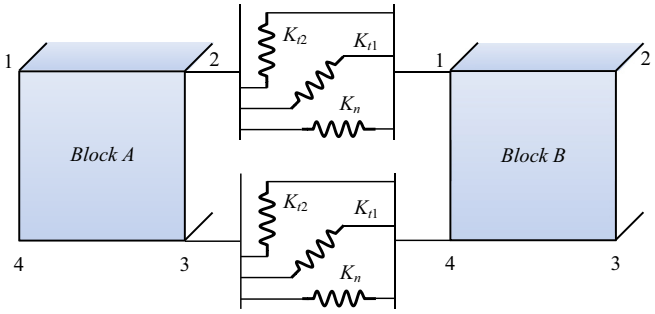

Fig. 5. Three-dimensional contacts in CDEM: contacts A2–B1 and A3–B4.

and DEM is used for the interface between adjacent blocks (Wang et al., 2013). A block element can be a four-node tetrahedron, a six-node wedge or an eight-node hexahedron. A three-dimensional contact, which connects two nodes of neighboring blocks, contains three joint springs (Li et al., 2015): one normal spring (K_n) and two tangential springs (K_{t1}, K_{t2}), as indicated in Fig. 6. These springs are orthogonal to each other, and their characteristics are the same as DEM (Li et al., 2004, 2015). With the breakable and sufficient springs in a contact, CDEM can accurately represent micro-cracking of rock masses.

3.2. Cracking criterion

The maximum tensile stress criterion and Mohr-Coulomb law are employed to describe the micro-cracks in brittle rock masses. Before strength criterion is applied to determine micro-cracking, spring forces in contact should be calculated (Li et al., 2015):

$$\begin{cases} F_n^j = -K_n^j \Delta u_n^j \\ F_t^j = -K_t^j \Delta u_t^j \end{cases} \tag{1}$$

where the superscript j means the jth spring; F_n, F_t stands for the normal and tangential spring force, respectively; K_n, K_t denote the normal and tangential stiffness, respectively; Δu_n, Δu_t represent the relative displacements in the normal and tangential directions, respectively.

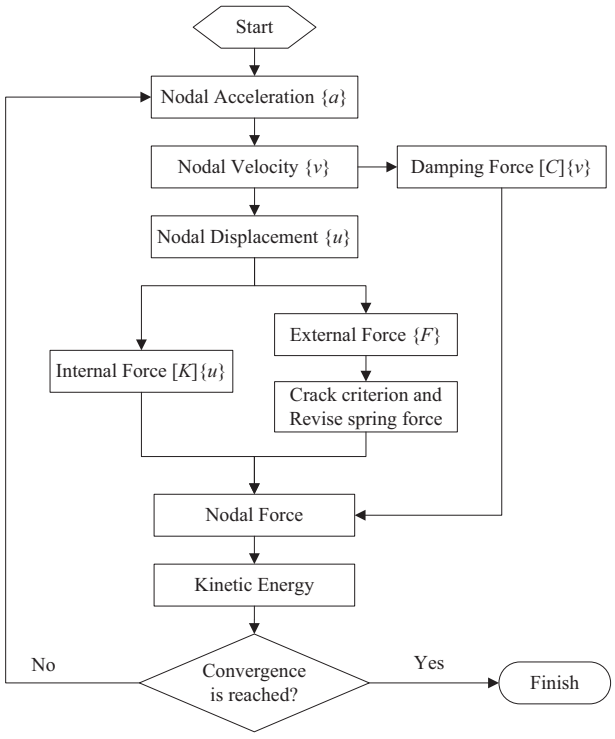

Fig. 6. Flow chart of the iteration process in CDEM.

The micro-cracks are initiated along the contact interface between two neighboring elements. For tensile or frictional cracks, the normal or frictional spring force should meet the following inequalities, respectively:

$$F_n \geqslant TA \tag{2}$$

$$F_t \geqslant cA + F_n \tan\varphi \tag{3}$$

where A is the nodal area; T stands for the maximum tensile strength; c, φ denote the cohesion and internal friction angle, respectively.

With the initialization of micro-cracks, rock material is changed from continuum into discontinuum. Thus, the normal or tangential spring force should be revised into:

$$F_n = 0 \text{ or } F_t = F_n \tan\varphi \tag{4}$$

3.3. Explicit CDEM procedure

The equations of solid deformation are obtained from equilibrium equations of all forces acting on the nodal masses, resulting in a system of equations of the following matrix form:

$$[M]^e\{\ddot{u}\}^e + [C]^e\{\dot{u}\}^e + [K]^e\{u\}^e = \{F\}^e_{\text{ext}} \tag{5}$$

where the superscript e means the element; $[M]$ stands for the diagonal mass matrix; $[C]$ is the damping matrix; $[K]$ denotes the stiffness matrix; $\{u\}$ means the vector of displacement; and $\{F\}_{\text{ext}}$ stands for the vector of external force, including the body force $\{F\}_b$, the spring force of contact $\{F\}_s$ (given by Eq. (3)) and the boundary traction $\{F\}_t$:

$$\{F\}^e_{\text{ext}} = \{F\}^e_b + \{F\}^e_s + \{F\}^e_t \tag{6}$$

CDEM utilizes a mixed explicit scheme for time integration. The acceleration is integrated by the central difference scheme while the velocity by the unilateral difference scheme. The schemes can be written as (Wang et al., 2013):

$$\{a\}^n = \{\ddot{u}\}^n = \frac{\{u\}^{n+1} - 2\{u\}^n + \{u\}^{n-1}}{(\Delta t)^2} \tag{7}$$

$$\{v\}^{n+1} = \{\dot{u}\}^{n+1} = \frac{\{u\}^{n+1} - \{u\}^n}{\Delta t} \tag{8}$$

where $\{a\}$, $\{v\}$, $\{u\}$ stand for acceleration, velocity and displacement, respectively; n means the nth time step; Δt is the time step interval. The explicit iteration scheme can be formulated from Eqs. (7) and (8) to the following form:

$$\{\dot{u}\}^{n+1} = \{\dot{u}\}^n + \{\ddot{u}\}^{n+1}\Delta t \tag{9}$$

$$\{u\}^{n+1} = \{u\}^n + \{\dot{u}\}^{n+1}\Delta t \tag{10}$$

The procedures of the explicit scheme for time stepping used in CDEM is illustrated in Fig. 7, which can be precisely summarized as follows (Wang et al., 2013):

- Calculate the external nodal forces $\{F\}^e_{\text{ext}}$ of the element e, which include the body forces, the possible spring forces from the neighboring elements and the tractions.
- Determine the micro-cracks based on the strength criterion. If micro-cracks occur, revise the spring forces based on Eq. (4).
- Calculate the internal nodal forces:

$$\{F\}^e_{\text{int}} = [K]^e\{u\}^e + [C]^e\{\dot{u}\}^e \tag{11}$$

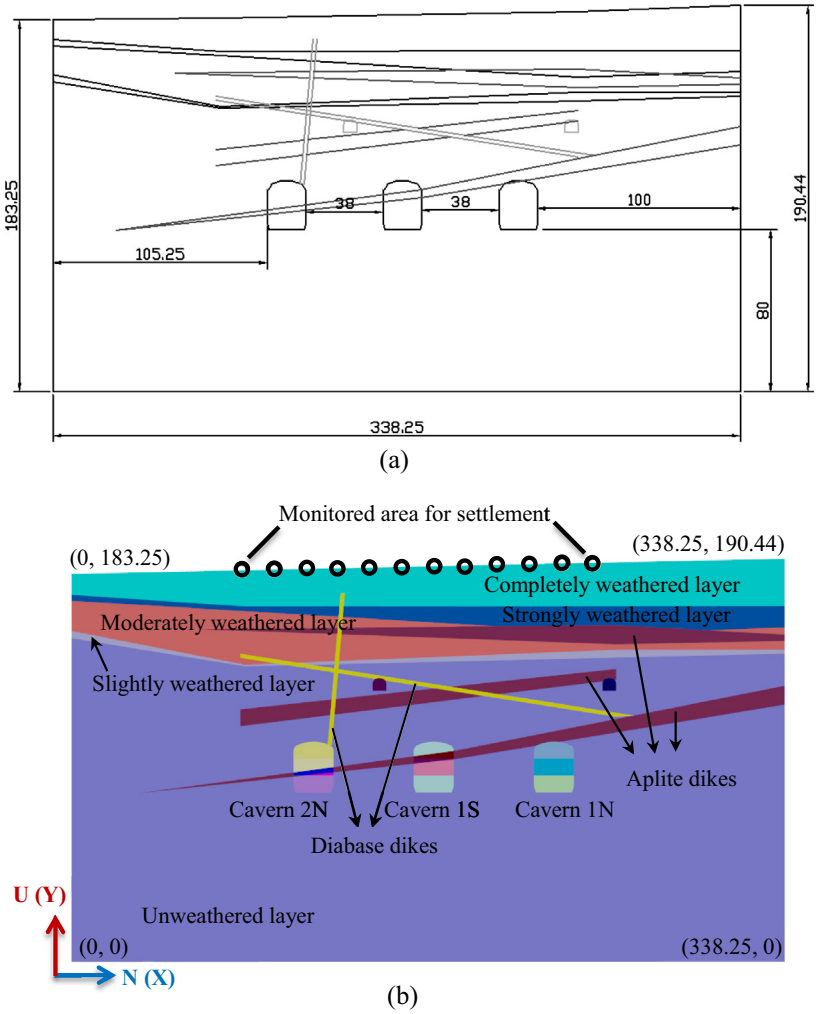

Fig. 7. Model representation of the studied profile: (a) profile from site investigation, and (b) established numerical model (unit: m).

- Calculate the total nodal forces $\{F\}^e_{\text{tot}}$:

$$\{F\}^e_{\text{tot}} = \{F\}^e_{\text{ext}} - \{F\}^e_{\text{int}} \tag{12}$$

- Calculate the nodal accelerations $\{a\}^e$ based on Newton's Second Law:

$$\{a\}^e = \{\ddot{u}\}^e = ([M]^e)^{-1}\{F\}^e_{\text{tot}} \tag{13}$$

- Calculate the nodal velocities $\{v\}^e$ and displacements $\{u\}^e$ by Eqs. (9) and (10), respectively.
- Calculate the total kinetic energy E_k of the system:

$$E_k = \sum_e \frac{1}{2}\{v\}^{eT}\{v\}^e \tag{14}$$

- Repeat the above procedures until the kinetic energy reaches a threshold.

Based on Courant–Friedrichs–Lewy (CFL) stability criterion, the critical time step is

$$t_{\text{cr}} = \frac{L_{\min}}{C_\rho}, \quad C_\rho = \sqrt{\frac{E}{\rho}} \tag{15}$$

where $L_{\min}$ is the minimum mesh size; C_ρ is the longitudinal wave speed; E is Young's modulus; ρ is density.

3.4. Verification of CDEM

CDEM was initially verified by modeling rock samples under uniaxial loading (Li et al., 2004). In their study, the numerical results from CDEM agreed well with the theoretical and experimental data. Zhang et al. (2005) validated CDEM for jointed rock simulations with a slope sliding experiment. The slope failure mode predicted by CDEM was similar to that obtained by experiments. Li et al. (2015) used the CDEM to predict the toppling failure of an opencast mine, and numerical results in micro-crack development were consistent with the GB-InSAR monitoring data. There are more detailed CDEM applications in several aspects of engineering reviewed by Li et al. (2008). Ma et al. (2011) and Wang et al. (2013) introduced the graphics processing unit-based parallelization of CDEM and extended its applications. In the present study, the validated CDEM was used to study the micro-crack development of surrounding masses near underground storage caverns.

4. An integrated platform of numerical simulation and microseismic monitoring

4.1. Numerical simulation with CDEM

According to site investigation, a model with different soil and rock layers is built, as shown in Fig. 7(a), with three storage

Table 1
Physical and mechanical properties of rock masses.

Rock mass	Parameter					
	Young's modulus E (GPa)	Poisson's ratio ν	Density ρ (kg/m^3)	Cohesion c (MPa)	Friction angle φ (°)	Tensile strength T (MPa)
Completely weathered granite	20	0.32	2550	0.8	25	0.6
Strongly weathered granite	25	0.28	2582	2.0	30	1.7
Moderately weathered granite	30	0.24	2614	3.0	35	2.5
Slightly weathered granite	35	0.20	2646	4.0	40	3.4
Unweathered granite	40	0.16	2678	6.0	45	4.0
Aplite dikes	30	0.20	2618	4.0	40	3.0
Diabase dikes	30	0.20	2788	0.8	25	0.6

Table 2
In-situ stresses in the studied site.

Depth (m)	Range of horizontal stress (MPa)	Average horizontal stress (MPa)	Vertical stress (MPa)
⩽65	3.14–5.52	3.82	Calculated as gravity stress by Eq. (16)
>65	3.63–9.02	6.17	

caverns, namely Cavern 1N, Cavern 1S and Cavern 2N. The studied profile has a dimension of about 338 m in length and of about 187 m in height. The rock masses are mainly granites, with some diabase and aplite dikes. The rock masses are composed of five layers, namely completely weathered layer, strongly weathered layer, moderately weathered layer, slightly weathered layer and unweathered layer. Despite the dikes, each layer consists of medium-grained or coarse-grained granite, with different weathering degrees. No large-scale fractures were found in this area. The physical and mechanical properties of the granites in different layers and dikes were obtained from site investigation and laboratory experiments (Lian, 2004), as indicated in Table 1. Some of the properties are rock mass properties while others are intact rock properties. They were provided by a survey and design institute in China. The gravity acceleration g is taken as 9.8 m/s^2. Besides, the *in-situ* stress field should be considered. As shown in Table 2, the horizontal in situ stress varies within a certain range. The average horizontal *in-situ* stress is adopted for numerical simulation. The vertical *in-situ* stress $\sigma_v(h)$ is calculated as:

$$\sigma_v(h) = \int_0^h \rho g dy \tag{16}$$

where h is the depth from the ground surface, and y is vertical.

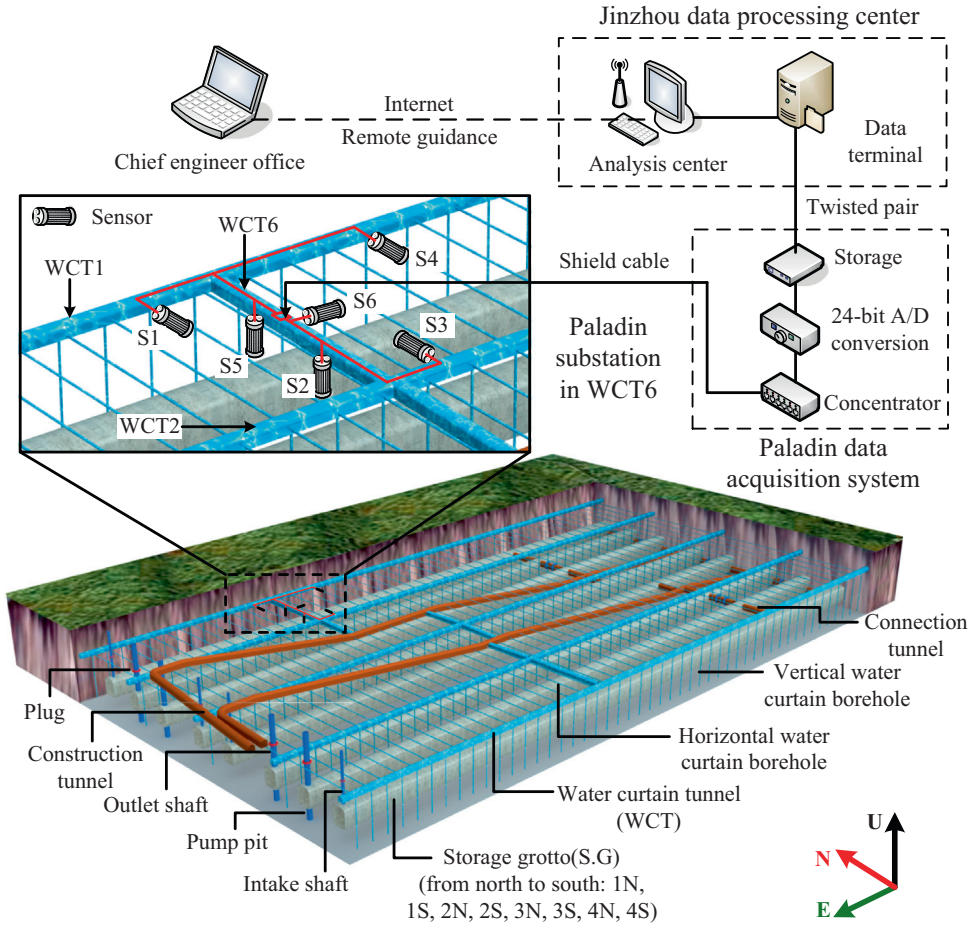

Fig. 8. The microseismic monitoring system installed in underground storage caverns in Jinzhou, Liaoning, China.

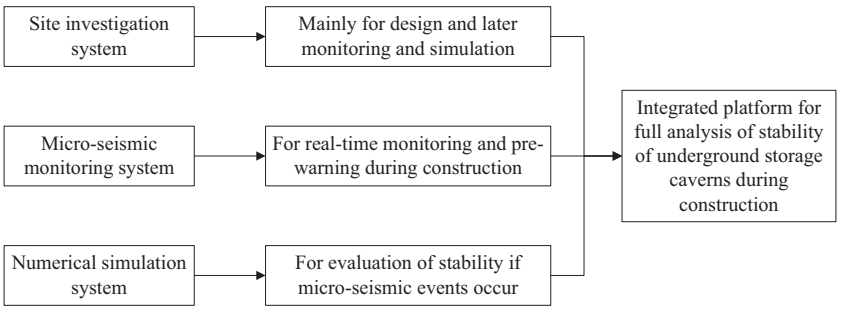

Fig. 9. The integrated platform for stability analysis of underground storage caverns during construction.

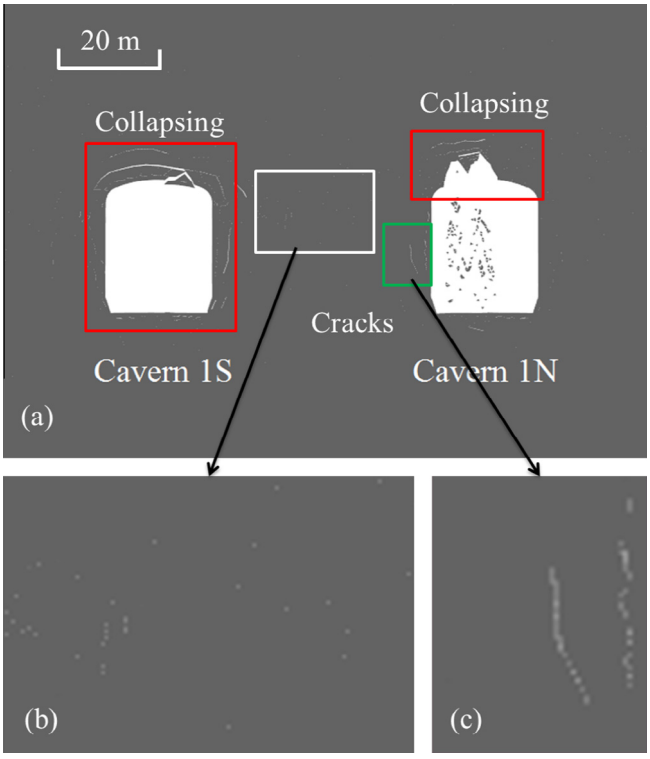

Fig. 10. Crack distribution by numerical simulation with CDEM: (a) an overall view, (b) magnified view of the micro-cracks, and (c) magnified view of the macro-cracks.

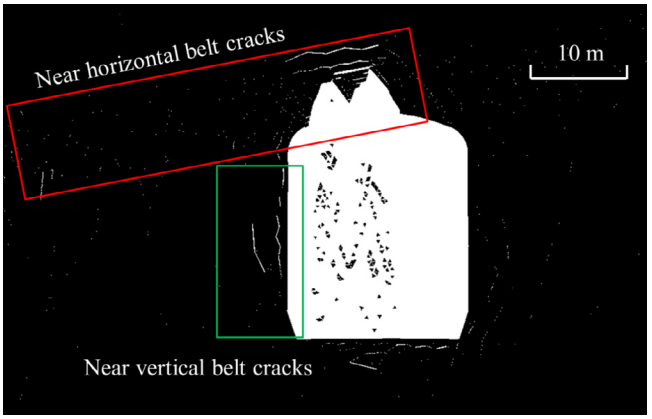

Fig. 11. Cracks distribution around Cavern 1N.

A pseudo 3D numerical model with wedge elements is used in this study, as shown in Fig. 7(b). The numerical model precisely describes the details of the studied area, including five granite layers and the diabase and aplite dikes. As can be seen that the aplite dikes just pass through the three storage caverns and the diabase dikes pass through the water curtain cavern. The primary crack distribution was characterized by the dykes with locations, sizes and directions. It is worth noting that the stability problem in this project was mainly caused by dikes near the caverns. As similar cases can hardly be found in the literature, the stability problem is much more concerning. Therefore, such a precise model is necessary.

The construction process of the storage caverns is simulated by this model. The cavern excavation was started from Cavern 1N and ended with Cavern 2S. Each storage cavern was sequentially excavated from the upper bench to the lower bench. Thus, a total number of nine excavation stages are simulated. Such extensive excavation might cause strong unloading effect. The CDEM can efficiently and accurately simulate the complex excavation process in order to reveal the unloading mechanisms and evaluate the stability of the storage caverns. It is should be mentioned that in the simulation the intersection of the cavern with the water curtain tunnel was not considered, since it was after the excavation process that we simulated. Thus, the unloading effect in the third dimension was much smaller than that of the other two dimensions and the 2D model is based on the plain strain concept.

4.2. Microseismic monitoring system

A state-of-the-art MS monitoring system, produced by ESG Company, was installed near the caverns, as shown in Fig. 8. It is mainly composed of several acceleration sensors, a Paladin signal acquisition system, and a Hyperion data processing system. The sensitivity of a single-component sensor is 30 v/g, with frequency ranging from 50 Hz to 5 kHz. The Paladin signal acquisition system, which uses analog-to-digital conversion and threshold triggering, has a sampling frequency of 20 kHz.

Considering the features of this project, a six-channel microseismic monitoring system was installed. Not only could the system perform real-time monitoring of micro-cracks, but also a stable and workable state can be ensured. The MS monitoring system covered the boxed area in Fig. 8, with a dimension of 300 m × 200 m × 100 m. The six acceleration sensors were arranged in a spatial array to monitor the microseismic events continuously. They are single-component sensors with a direction, which depends on the dip angle they are put. With different dip angles, the sensors can receive microseismic signals from different directions, as shown in Fig. 8. Several methods such as threshold

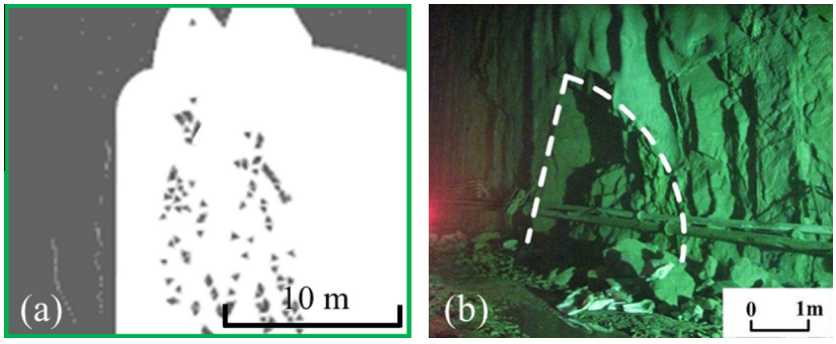

Fig. 12. Rock collapses around the south face of Cavern 1N from (a) numerical simulation, and (b) site investigation.

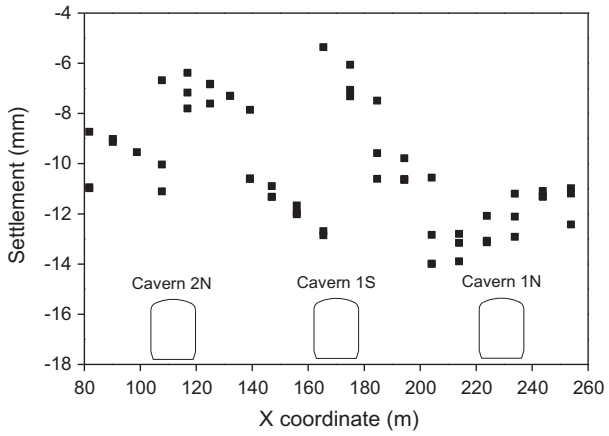

Fig. 13. Surface settlement after excavation by CDEM.

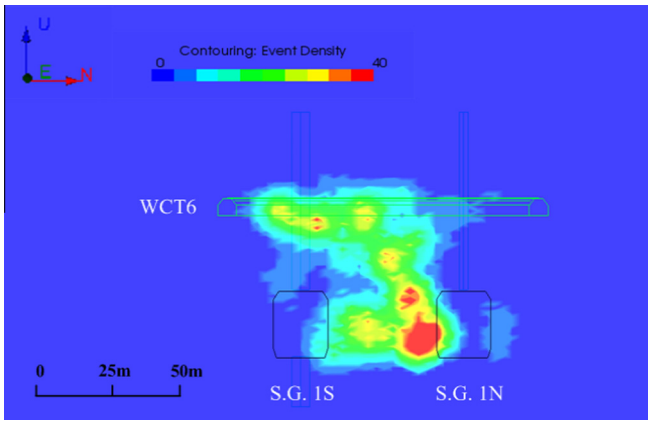

Fig. 15. Microseismic events around Caverns 1N and 1S.

setting, filtering and bandwidth detection were applied to identify the waveform and store the spectral analysis chart (Ma et al., 2013).

4.3. The integrated platform

The site investigation, microseismic monitoring and numerical simulation systems are integrated into a uniform platform for comprehensive stability analysis of underground storage caverns during construction, as indicated in Fig. 9. The site investigation system aims at the design of the underground storage caverns primarily, and it also provides information on the location for microseismic monitoring and the model for numerical simulation. The microseismic monitoring system provides real-time data of microseismic events and pre-warns the possible threats to the stability of the underground storage caverns. If any possibly-threatening events occur, numerical simulation will be performed for further analysis.

5. Results and discussions

5.1. Numerical simulation results

The crack distribution after excavation and unloading obtained by the CDEM simulation is presented in Fig. 10. Generally, the cracks are distributed in mainly four areas, as shown in Fig. 10(a), including the areas surrounding the two caverns and between them. As indicated by site investigation, some diabase and aplite dikes pass through these areas. The cracks were mainly caused by the dikes after unloading. Similar conclusions can be drawn from the microseismic monitoring results.

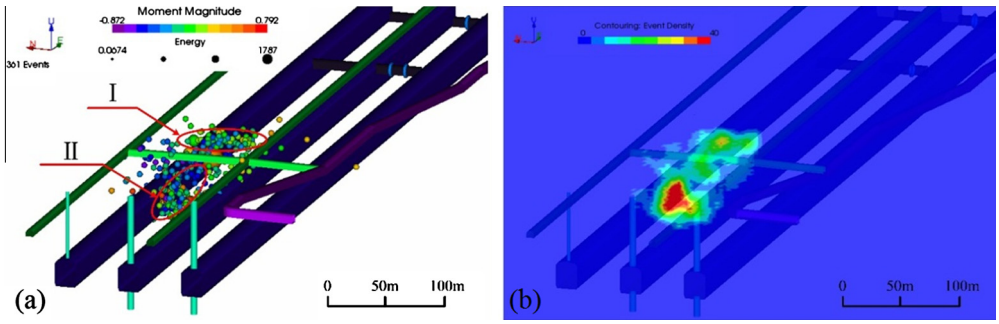

Fig. 14. The spatial distribution of microseismic events from July 28 to August 26, 2014: (a) distribution of microseismic events, and (b) density of microseismic events.

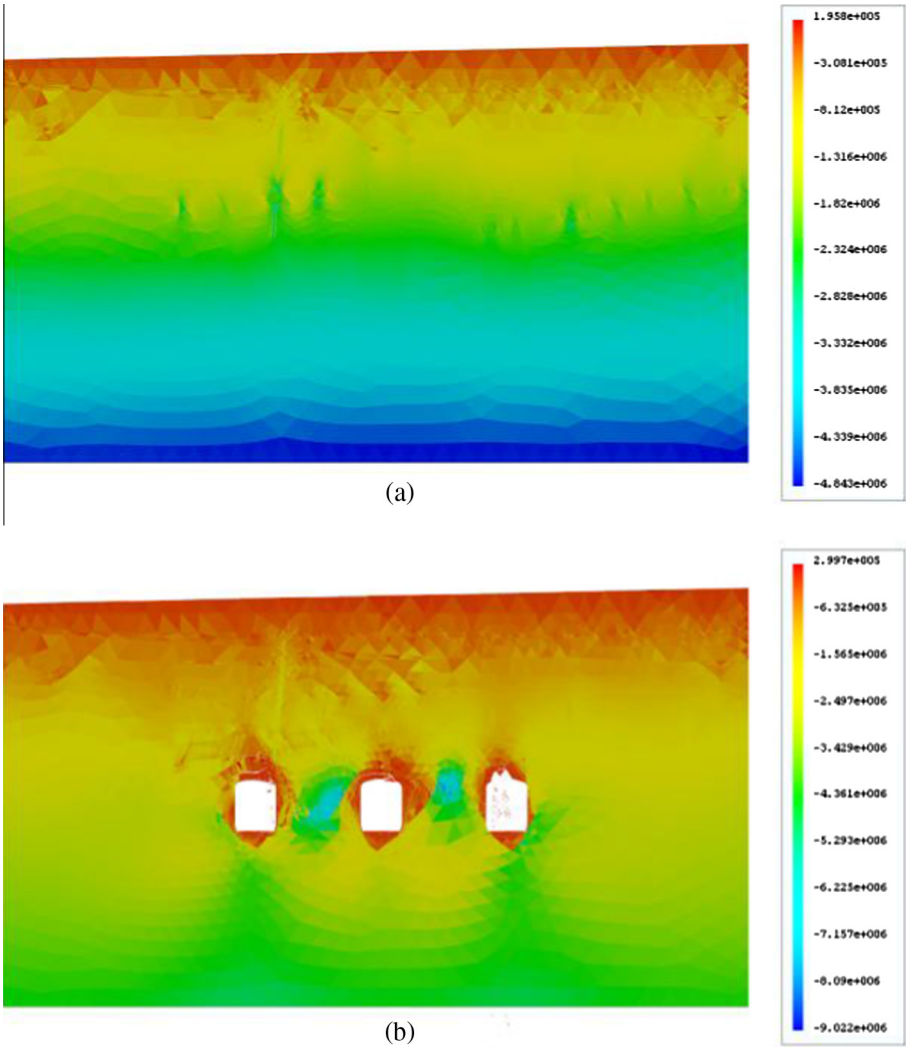

Fig. 16. Stress transfer after excavation (unit: Pa): (a) initial *y*-stress field, and (b) *y*-stress field after excavation.

A closer view on Cavern 1N is illustrated in Fig. 11, which clearly shows two main belt areas of the cracks, as indicated by the red[1] and green boxes. The cracks in an approximately horizontal belt mainly appear above the cavern, while the cracks in an approximately vertical belt appear around the south face of Cavern 1N. The red box shows some micro-cracks while the green box shows some macro-cracks. Despite the rock collapse from the cavern roof, most rocks in the red box are damaged without significant cracking. However, the rocks in the green box are apparently cracked due to the unloading effect. The red color indicates the area with most cracks, similar with the green-boxed area in Fig. 11. Numerical simulation also indicates that the rock collapses occur around the south face of Cavern 1N, as shown in Fig. 12(a). The phenomenon was verified by field observation, as shown in Fig. 12(b). It is caused by the unloading effect under excavation, which results in higher stresses in this area. When the stress is greater that the strength of the surrounding rock masses, cracking occurs and the elastic energy stored in the rock masses is released.

The surface settlement can also be obtained from numerical simulation, as indicated in Fig. 13. The monitored points for surface settlement are shown in Fig. 7(b), with a range of *X* coordinates from 80 m to 260 m. Located above the three storage caverns, the monitored points record the deformation of the rock masses after excavation of the storage caverns. From the figure, we learn that the settlements range from about 6 mm to about 14 mm and the average settlement is about 10 mm. The largest settlements are from the area between Cavern 1N and Cavern 1S, which means this area takes the most risk of local instability of the surrounding rock masses. A similar conclusion can be drawn from the microseismic monitoring data. Thus, the surface settlements can also be used as an indicator to evaluate the cavern stability.

5.2. Microseismic monitoring results

Since July 28, 2014 when the MS monitoring system was set up, 492 valid microseismic events had been detected till August 26, 2014, including 361 micro-cracking events, 123 blasting events and 8 striking events. The micro-cracks caused by excavation and unloading were mainly distributed in Caverns 1N and 1S and regions nearby, in two belt areas as indicated in Fig. 14(a). One is nearly horizontal and located at Chainage 2 + 63; the other is nearly vertical and located between Chainage 2 + 40 and 2 + 60. The microseismic events mainly concentrate in the two belt areas, with the largest density at Chainage 2 + 40 ~ 2 + 60, as shown in Fig. 14(b). The area with the largest density was the most dangerous area. The rocks are apparently cracked due to the unloading effect, as shown in Fig. 15, which is similar with numerical results

[1] For interpretation of color in Fig. 11, the reader is referred to the web version of this article.

in Fig. 11. Meanwhile, the unloading effect leads to redistribution of the stress field around the rock masses, and the stress is transferred into the diabase and aplite dikes (Fig. 16). The stress transfer causes more micro-cracks, and the belt areas of cracking are formed (Figs. 10–12). Continuous excavation is the main cause for the damage of the dikes and local instability of the surrounding rock masses.

5.3. Discussions

Nevertheless, the progressive damage and failure evolution of underground water-sealed storage caverns has not been understood well, nor their damage and failure mechanisms. The method of CDEM provided a means to understand the progressive damage and failure evolution, and damage and failure mechanisms for large-scale underground excavations. In fact, the CDEM can also simulate purely continuous or purely discontinuous problems, such as elastoplastics and rock joints, like the FEM or the DEM does. What makes the CDEM more powerful is that the CDEM introduces cracking mechanism, which can reproduce the progressive failure process of a material from continuum to discontinuum. Thus, the CDEM is capable of simulating damage, crack growth and failure problems, which is of great significance in engineering applications. More generally, the CDEM can well simulate the failure state of materials regardless of joint distribution and size effect (Li et al., 2005, 2007). Besides, the graphics processing unit-based parallelization makes CDEM capable of undertaking large-scale computing tasks in engineering levels (Ma et al., 2011; Wang et al., 2013). However, the CDEM has its limitations in the simulations for underground storage caverns as it cannot estimate the damage or cracking time well. Additionally, the fluid flow effects in rock masses and fractures are not considered in CDEM (Wang et al., 2015a). The improvements for CDEM are being further performed.

6. Conclusions

In this study, the stability of an underground storage cavern project has been analyzed. Microseismic (MS) events and micro-crack evolution were investigated through an integrated platform, which included a novel numerical method named Continuous–Discontinuous Element Method (CDEM) and a six-channel MS monitoring system. More specifically, CDEM was presented to model the micro-cracks due to excavation unloading, and the MS system was introduced to monitor real-time MS events of the storage caverns under construction. Meanwhile, numerical results were validated using MS monitoring data. The following conclusions can be drawn:

(1) The integration of CDEM and MS monitoring system was proved to be successful in capturing micro-cracks in underground storage caverns. The cracking areas obtained by CDEM agreed well with MS monitoring data. Micro-cracks were mainly located in two belt areas, i.e., one was approximately horizontal and the other was approximately vertical. The MS events were mainly distributed in the two belt areas, and the similar phenomenon was reproduced by CDEM simulation.

(2) Numerical simulation indicated that rock collapses around the south face of Cavern 1N were in good agreement with field observation, which were caused by excavation unloading and stress redistribution. High stresses led to cracking of rock masses and release of elastic energy, and continuous excavation led to the damage of the dikes and local instability of surrounding rock masses. Moreover, the stress field around the cavern was redistributed and transferred into the diabase and aplite dikes, and therefore more micro-cracks in the belt areas were formed.

(3) Numerical results provided the settlement of underground cavern after excavation for stability assessment. The settlement indicated that the area between Cavern 1N and Cavern 1S undergone the most risk of local instability of surrounding rock masses, which could be used as an indicator for stability assessment and risk prediction.

Acknowledgements

The authors are grateful for the financial support from the National Natural Science Foundation of China (Grant No. 51504233), the China Post Doctoral Fund Project (Grant No. 2015M571137) and the National Basic Research Program of China (973 Program, Grant No. 2014CB047100).

References

Åberg, B., 1977. Prevention of gas leakage from unlined reservoir in rock. In: Proc. 1st Int. Symposium on Storage in Excavated Rock Caverns, Stockholm, Sweden.
Benardos, A.G., Kaliampakos, D.G., 2005. Hydrocarbon storage in unlined rock caverns in Greek limestone. Tunn. Undergr. Sp. Technol. 20 (2), 175–182.
Bergman, S.M., 1984. Underground storage of oil and gas. J. Energy Eng. 110 (3), 181–190.
Broms, B.B., Zhao, J., 1993. Potential use of underground caverns in Singapore. In: Proc. Seminar on Rock Caverns for Underground Space Utilization. Nanyang Technological University, Singapore, pp. 11–21.
Cai, M., Kaisera, P.K., Moriokab, H., Minamib, M., Maejimab, T., Tasakac, Y., Kurosec, H., 2007. FLAC/PFC coupled numerical simulation of AE in large-scale underground excavations. Int. J. Rock Mech. Min. Sci. 44, 550–564.
Cai, W., Dou, L., Li, Z., He, J., He, H., Ding, Y., 2015. Mechanical initiation and propagation mechanism of a thrust fault: a case study of the Yima section of the Xiashi-Yima thrust (north side of the eastern Qinling Orogen, China). Rock Mech. Rock Eng. 48 (5), 1927–1945.
Chen, H.M., Zhao, Z.Y., Sun, J.P., 2013. Coupled hydro-mechanical model for fractured rock masses using the discontinuous deformation analysis. Tunn. Undergr. Sp. Technol. 38, 506–516.
Cundall, P.A., 1971. A computer model for simulating progressive large scale movements in blocky rock systems. In: Proc. Symp. Rock Fracture (ISRM), vol. 1, Paper No. II–8, Nancy, France.
Cundall, P.A., Strack, O.D., 1979. A discrete numerical model for granular assemblies. Géotechnique 29 (1), 47–65.
Feng, G.L., Feng, X.T., Chen, B.R., Xiao, Y.X., Jiang, Q., 2015. Sectional velocity model for microseismic source location in tunnels. Tunn. Undergr. Sp. Technol. 45, 73–83.
Feng, X.T., Yu, Y., Feng, G.L., Xiao, Y.X., Chen, B.R., Jiang, Q., 2016. Fractal behaviour of the microseismic energy associated with immediate rockbursts in deep, hard rock tunnels. Tunn. Undergr. Sp. Technol. 51, 98–107.
Gnirk, P.F., Fossum, A.F., 1979. On the formulation of stability and design criteria for compressed air energy storage in hard rock caverns. In: 14th Intersociety Energy Conversion Engineering Conference, vol. 1, pp. 429–440.
Goodall, D.C., Åberg, B., Breke, T.L., 1988. Fundamentals of gas containment in unlined rock caverns. Rock Mech. Rock Eng. 21 (4), 235–258.
He, L., Zhang, Q.B., 2015. Numerical investigation of arching mechanism to underground excavation in jointed rock mass. Tunn. Undergr. Sp. Technol. 50, 54–67.
Heusermann, S., Rolfs, O., Schmidt, U., 2003. Nonlinear finite-element analysis of solution mined storage caverns in rock salt using the LUBBY2 constitutive model. Comput. Struct. 81, 629–638.
Hong, J.S., Lee, H.S., Lee, D.H., Kim, H.Y., Choi, Y.T., Park, Y.J., 2006. Microseismic event monitoring of highly stressed rock mass around underground oil storage caverns. Tunn. Undergr. Sp. Technol. 21 (3), 292–297.
Ibrahim, E., Soubra, A.H., Mollon, G., Raphael, W., Dias, D., Reda, A., 2015. Three-dimensional face stability analysis of pressurized tunnels driven in a multilayered purely frictional medium. Tunn. Undergr. Sp. Technol. 49, 18–34.
Jing, L.R., Stephansson, O., 2007. Fundamentals of Discrete Element Methods for Rock Engineering: Theory and Applications. Elsevier.
Kaiser, P.K., 2009. Seismic hazard evaluation in underground construction. In: Proceedings of the 7th International Symposium on Rockburst and Seismicity in Mines (RaSiM7). Rinton Press, New York, pp. 1–26.
Kiyoyama, S., 1990. The present state of underground crude oil storage technology in Japan. Tunn. Undergr. Sp. Technol. 5 (4), 343–349.
Koyama, T., Li, B., Jiang, Y., Jing, L., 2009. Numerical modelling of fluid flow tests in a rock fracture with a special algorithm for contact areas. Comput. Geotech. 36, 291–303.
Lee, C.I., Song, J.J., 2003. Rock engineering in underground energy storage in Korea. Tunn. Undergr. Sp. Technol. 18 (5), 467–483.
Lee, H.S., Lee, D.H., Kim, H.Y., Choi, Y.T., 2006. Design criteria for thermo-mechanical stability of rock mass around lined rock cavern for underground LNG storage. Tunn. Undergr. Sp. Technol. 21 (3–4), 337.

Li, S.H., Zhao, M.H., Wang, Y.N., Rao, Y., 2004. A new numerical method for DEM-block and particle model. Int. J. Rock Mech. Min. Sci. 41 (3), 436.
Li, S.H., Lian, Z.Z., Wang, J.G., 2005. Effect of rock mass structure and block size on the slope stability—physical modeling and discrete element simulation. Sci. China Ser. E Eng. Mater. Sci. 48 (1), 1–17.
Li, S.H., Wang, J.G., Liu, B.S., Dong, D.P., 2007. Analysis of critical excavation depth for a jointed rock slope using a face-to-face discrete element method. Rock Mech. Rock Eng. 40 (4), 331–348.
Li, S.H., Liu, X.Y., Liu, T.P., Feng, C., 2008. Continuum-based discrete element method and its applications. In: Proceedings of UK-China Summer School/International Symposium on DEM, Beijing, China, pp. 147–170.
Li, S.C., Wang, Z.C., Ping, Y., Zhou, Y., Zhang, L., 2014. Discrete element analysis of hydro-mechanical behavior of a pilot underground crude oil storage facility in granite in China. Tunn. Undergr. Sp. Technol. 40, 75–84.
Li, Z., Wang, J.A., Li, L., Wang, L.X., Liang, R.Y., 2015. A case study integrating numerical simulation and GB-InSAR monitoring to analyze flexural toppling of an anti-dip slope in Fushun open pit. Eng. Geol. 197, 20–32. http://dx.doi.org/10.1016/j.enggeo.2015.08.012.
Lian, J.F., 2004. The research of rock mass integrity parameters and surrounding rock mass stability evaluation on a huge LPG cavern with water sealing in Jinzhou. Doctoral dissertation, China University of Geosciences, Beijing, China (in Chinese).
Lindblom, U.E., 1997. Design criteria for the Brooklyn Union gas storage caverns at JFK airport, New York. Int. J. Rock Mech. Min. Sci. 34 (3–4), Paper No. 179.
Lisjak, A., Grasselli, G., Vietor, T., 2014. Continuum–discontinuum analysis of failure mechanisms around unsupported circular excavations in anisotropic clay shales. Int. J. Rock Mech. Min. Sci. 65, 96–115.
Lisjak, A., Garitte, B., Grasselli, G., Müller, H.R., Vietor, T., 2015. The excavation of a circular tunnel in a bedded argillaceous rock (Opalinus Clay): short-term rock mass response and FDEM numerical analysis. Tunn. Undergr. Sp. Technol. 45, 227–248.
Lu, M., 1998. Finite element analysis of a pilot gas storage in rock cavern under high pressure. Eng. Geol. 49 (3–4), 353–361.
Ma, Z.S., Feng, C., Liu, T.P., Li, S.H., 2011. A GPU accelerated continuous-based discrete element method for elastodynamics analysis. Adv. Mater. Res. 320, 329–334.
Ma, K., Tang, C.A., Li, L.C., Li, H., Xu, N.W., Xiao, P., Yang, J.Y., 2013. The effect analysis of the Dagangshan right bank slope anti-shear tunnel reinforcement based on microseismic monitoring and numerical analysis. Chin. Rock Soil Mech. 32 (6), 1239–1247 (in Chinese).
Mahabadi, O.K., Cottrell, B.E., Grasselli, G., 2010. An example of realistic modelling of rock dynamics problems: FEM/DEM simulation of dynamic Brazilian test on Barre granite. Rock Mech. Rock Eng. 43 (6), 707–716.
Mahabadi, O.K., Lisjak, A., Grasselli, G., Munjiza, A., 2012. Y-Geo: a new combined finite-discrete element numerical code for geomechanical applications. Int. J. Geomech. 12, 676–688.
Mandal, A., Chakravarthy, C., Nanda, A., Rath, R., Usmani, A., 2013. Analysis and design approach for large storage caverns. Int. J. Geomech. 13 (1), 69–75.
Mohanty, S., Vandergrift, T., 2012. Long term stability evaluation of an old underground gas storage cavern using unique numerical methods. Tunn. Undergr. Sp. Technol. 30, 145–154.
Morfeldt, C.O., 1974. Storage of Oil and Gas in Unlined Caverns. HC 39: 74. Reprint Society of Engineers of AIME, Amsterdam, Netherlands.
Morfeldt, C.O., 1983. Storage of petroleum products in man-made caverns in Sweden. Bull. Int. Assoc. Eng. Geol. 28 (1), 17–30.
Munjiza, A., 2004. The Combined Finite-Discrete Element Method. John Wiley & Sons Ltd., Chichester, West Sussex, England.
Munjiza, A., Owen, D.R.J., Bicanic, N., 1995. A combined finite-discrete element method in transient dynamics of fracturing solids. Eng. Comput. 12, 145–174.
Nadimi, S., Shahriar, K., Sharifzadeh, M., Moarefvand, P., 2011. Triaxial creep tests and back analysis of time-dependent behavior of Siah Bisheh cavern by 3-dimensional distinct element method. Tunn. Undergr. Sp. Technol. 26 (1), 155–162.
Narasimhan, T.N., Witherspoon, P.A., 1976. An integrated finite difference method for analyzing fluid flow in porous media. Water Resour. Res. 12, 57–64.
Park, J.J., Jeon, S., Chung, Y.S., 2005. Design of Pyongtaek LPG storage terminal underneath Lake Namyang: a case study. Tunn. Undergr. Sp. Technol. 20 (5), 463–478.
Preece, D.S., Foley, J.T., 1983. Finite-element analysis of salt caverns employed in the Strategic Petroleum Reserve. No. SAND-82-1205C. CONF-830511-1. Sandia National Labs., Albuquerque, NM, USA.
Rutqvist, J., Kim, H.M., Ryu, D.W., Synn, J.H., Song, W.K., 2012. Modeling of coupled thermodynamic and geomechanical performance of underground compressed air energy storage in lined rock caverns. Int. J. Rock Mech. Min. Sci. 52, 71–81.
Shi, G.H., 1988. Discontinuous Deformation Analysis – A New Numerical Model for the Static and Dynamics of Block Systems. PhD Dissertation, Department of Civil Engineering, UC Berkeley.
Sun, J.P., Zhao, Z.Y., 2010. Effects of anisotropic permeability of fractured rock masses on underground oil storage caverns. Tunn. Undergr. Sp. Technol. 25 (5), 629–637.
Sun, J.P., Zhao, Z.Y., Zhang, Y., 2011. Determination of three dimensional hydraulic conductivities using a combined analytical/neural network model. Tunn. Undergr. Sp. Technol. 26 (2), 310–319.
Tang, C.A., Wang, J.M., Zhang, J.J., 2011. Preliminary engineering application of microseismic monitoring technique to rockburst prediction in tunneling of Jinping II project. J. Rock Mech. Geotech. Eng. 2 (3), 193–208.
Tezuka, M., Seoka, T., 2003. Latest technology of underground rock cavern excavation in Japan. Tunn. Undergr. Sp. Technol. 18 (2–3), 127–144.
Thunvik, R., Braester, C., 1980. Modelling of ground water flow around oil storage caverns. Appl. Math. Model. 4 (3), 225–227.
Wang, L.X., Li, S.H., Zhang, G.X., Ma, Z.S., Zhang, L., 2013. A GPU-based parallel procedure for nonlinear analysis of complex structures using a coupled FEM/DEM approach. Math. Probl. Eng., 1–15 http://dx.doi.org/10.1155/2013/618980 618980.
Wang, L.X., Li, S.H., Ma, Z.S., Feng, C., 2015a. A cell-centered finite volume method for fluid flow in fractured porous media and its parallelization with OpenMP. Chin. J. Rock Mech. Eng. 34 (5), 865–875 (in Chinese).
Wang, Z.C., Li, S.C., Qiao, L.P., Zhang, Q.S., 2015b. Finite element analysis of the hydro-mechanical behavior of an underground crude oil storage facility in granite subject to cyclic loading during operation. Int. J. Rock Mech. Min. Sci. 73, 70–81.
Xu, N.W., Tang, C.A., Li, L.C., Zhou, Z., Sha, C., Liang, Z.Z., Yang, J.Y., 2011. Microseismic monitoring and stability analysis of the left bank slope in Jinping first stage hydropower station in southwestern China. Int. J. Rock Mech. Min. Sci. 48 (6), 950–963.
Yang, M.J., Guan, B.S., 2001. Theoretical and numerical simulation study of underground gas-storage caverns with water curtain. Chin. J. Rock Mech. Eng. 20 (3), 301–305 (in Chinese).
Yang, H.S., Kang, J.G., Kim, K.S., Kim, C.S., 2004. Groundwater flow characterization in the vicinity of the underground caverns in fractured rock masses by numerical modeling. Geosci. J. 8 (4), 401–413.
Yang, T.H., Jia, P., Shi, W.H., Wang, P.T., Liu, H.L., Yu, Q.L., 2014. Seepage–stress coupled analysis on anisotropic characteristics of the fractured rock mass around roadway. Tunn. Undergr. Sp. Technol. 43, 11–19.
Zhang, L., Wei, Z.A., Liu, X.Y., Li, S.H., 2005. Application of three-dimensional discrete element face-to-face contact model with fissure water pressure to stability analysis of landslide in Panluo iron mine. Sci. China Ser. E Eng. Mater. Sci. 48 (1), 146–156.
Zhao, J., Choa, V., Broms, B.B., 1996. Construction and utilization of rock caverns in Singapore Part B: development costs and utilization. Tunn. Undergr. Sp. Technol. 11 (1), 73–79.
Zhao, J., Liu, Q., Lee, K.W., Choa, V., Teh, C.I., 1999a. Underground cavern development in the Jurong sedimentary rock formation. Tunn. Undergr. Sp. Technol. 14 (4), 449–459.
Zhao, J., Zhou, Y.X., Hefny, A.M., Cai, J.G., Chen, S.G., Li, H.B., Liu, J.F., Jain, M., Foo, S.T., Seah, C.C., 1999b. Rock dynamics research related to cavern development for ammunition storage. Tunn. Undergr. Sp. Technol. 14 (4), 513–526.
Zhao, J., Ng, W.L., Cai, J.G., Zhang, X.H., Bian, H.Y., 2004. Feasibility of underground hydrocarbon storage caverns at Jurong Island. Tunn. Undergr. Sp. Technol. 19 (4–5), 364.
Zhu, W.S., Zhao, J., 2004. Stability Analysis and Modelling of Underground Excavations in Fractured Rocks. Elsevier, p. 308, ISBN 978-0-08-043012-6.
Zhu, W.S., Li, X.J., Zhang, Q.B., Zheng, W.H., Xin, X.L., Sun, A.H., Li, S.C., 2010. A study on sidewall displacement prediction and stability evaluations for large underground power station caverns. Int. J. Rock Mech. Min. Sci. 47 (7), 1055–1062.